Applied Catalysis B: Environmental 148–149 (2014) 436–445

Contents lists available at ScienceDirect

Applied Catalysis B: Environmental

journal homepage: www.elsevier.com/locate/apcatb

# Identification of the coke deposited on an HZSM-5 zeolite catalyst during the sequenced pyrolysis–cracking of HDPE

M. Ibáñez, M. Artetxe, G. Lopez, G. Elordi, J. Bilbao, M. Olazar, P. Castaño*

*Department of Chemical Engineering, University of the Basque Country (UPV/EHU), P O Box 644, 48080 Bilbao, Spain*

ARTICLE INFO

*Article history:*
Received 17 October 2013
Received in revised form 8 November 2013
Accepted 13 November 2013
Available online 21 November 2013

*Keywords:*
Coke deactivation
MFI zeolite
Light olefins
Plastic valorization
Spectroscopy

ABSTRACT

The pyrolysis–cracking of high-density polyethylene (HDPE) has been studied in two sequenced steps: (1) flash pyrolysis in a conical spouted bed reactor, and (2) catalytic cracking of the volatiles (waxes) in a fixed bed reactor containing a HZSM-5 zeolite catalyst, aiming light olefins as final products. The pyrolysis and cracking have been carried out isothermally at 500 °C, with a continuous feed of HDPE (1 g $min^{-1}$) for up to 5 h (300 g of HDPE fed). We have correlated the catalytic deactivation by coke (carbonaceous deposits), in terms of amount and composition, with the profiles of gas composition along time on stream and space time. The amount and composition of coke in three axial positions of the catalytic bed have been elucidated using thermogravimetric (TG-TPO) and spectroscopic techniques ($^{13}C$ CP-MAS NMR, Raman, FTIR, FTIR-TPO-MS and FTIR-pyridine). Our results show that there are two pathways of coke formation: (i) initiation, during the first hour on stream and particularly in the inlet of the catalytic reactor; and (ii) steady coke formation, after the first hour on stream which is more severe in the last axial position of the catalytic reactor. The initiation step stems from the degradation of the waxes produced in the pyrolysis of HDPE and causes a dropping in the mesopore area of the catalyst. The steady coke formation step is caused by the condensation of light olefins and causes the degradation of the micropore area and the Brønsted acidity of the catalyst.



## 1. Introduction

The consumption of plastic products is increasing every year and accounts for over 100 kg per person per year in industrialized countries. These materials, from which polyolefins are the main fractions, generate an environmental problem that has driven urgent recycling concern [1,2]. Pyrolysis or thermal cracking of polyolefins is a tertiary recycling route that is attractive for obtaining fuels or high added value chemicals [3–5]. The pyrolysis requires temperatures of 500–700 °C and the selectivity of the products is determined by the operating conditions [6,7]. The performance of the process may be improved by the incorporation of a cracking catalyst, which leads to a change of the scission mechanism, decreasing the apparent activation energy and consequently the operating temperature required, and increasing the selectivity of the valued products [8–10]. The pyrolysis and catalytic cracking may take place in a single reactor (simultaneous pyrolysis–cracking) or in two reactors in series (sequenced pyrolysis–cracking). The later option allows optimizing the operating conditions of pyrolysis and catalytic cracking separately, which leads to overall improvement of the efficiency of the process [11–13].

The fluidized bed reactor is the most developed technology for polyolefin pyrolysis and for simultaneous pyrolysis–cracking due to its high heat and mass transfer rates, ensuring isothermal conditions [14–17], which is the major difficulty to overcome owing to the low thermal conductivity of polyolefins. The simultaneous pyrolysis–cracking of polyolefins takes place according to the following steps: (i) melting; (ii) volatilization; (iii) thermal cracking; and (iv) catalytic cracking. The vigorous cyclic movement characteristic of the conical spouted bed reactor helps the initial two steps and avoids bed defluidization [18]. This defluidization is caused by the agglomeration of the bed particles covered with the melted polyolefins. Furthermore, high heat and mass transfer rates are attained, [19] which leads to a fast volatilization of the melted polyolefins. Furthermore, the low residence time of the gases [20] avoids undesirable reactions during thermal or catalytic cracking [21,22]. Thus, the conical spouted bed reactors are highly versatile and, furthermore, use of a cracking catalyst with specific acidity and shape selectivity increases the selectivity of the valued products [21,23,24].

The catalysts most frequently used in the pyrolysis–cracking are zeolites (Hβ, HY, mordenite, HZSM-5), ordered mesoporous aluminosilicates (Al-MCM-41 and Al-SBA-15), clays and equilibrated

* Corresponding author. Tel.: +34 94 601 8435; fax: +34 94 601 3500.
*E-mail address:* pedro.castano@ehu.es (P. Castaño).

0926-3373/$ – see front matter © 2013 Elsevier B.V. All rights reserved.
http://dx.doi.org/10.1016/j.apcatb.2013.11.023

FCC catalysts [24–30]. The HZSM-5 zeolite catalyst has a unique performance in terms of olefin selectivity and lifetime [28,31,32], due to the following intrinsic features [33,34]: (i) moderate acid strength of the catalytic sites, (ii) micropores with a suitable dimensions for inhibiting the formation of large molecules ($C_{20+}$), (iii) very high porosity and connectivity between the pores, which favor the diffusion of reactants, products and by-products, and (iv) the absence of "cages" at the intersections of the pores. The main source of catalytic deactivation of HZSM-5 zeolites during the pyrolysis–cracking of polyolefins is carbonaceous deposit formation, typically known as coke, which blocks the accessibility of the reactants towards the acid sites [28,29,32,35,36].

Our previous works contributed to understand the mechanisms of catalytic deactivation in the simultaneous pyrolysis–cracking of HDPE [28,29,32], recognizing two types of coke [32]: coke I, deposited on the surface of the zeolite crystals, amorphous and containing long aliphatic chains, and coke II, primarily aromatic, structured and condensed, deposited on both the interior and the exterior of the zeolite crystals. In this work, we have investigated the precursors of each pathway and each type of coke formed on the catalyst, aiming strategies for a rational control of coke deposition. Thus, we have studied the deactivation of HZSM-5 zeolite in the second step of the sequenced pyrolysis–cracking process. This step has been performed into a fixed bed reactor divided in three sub-beds with identical amount of catalyst; this will enable to establish a correlation between the concentration of species in the gas phase (no liquid phase whatsoever in this second step) with the rate of formation and nature of the coke.

## 2. Experimental

### 2.1. Reaction and product analysis equipment

The high-density polyethylene (HDPE) is the third-largest commodity plastic material in the world, after polyvinyl chloride and polypropylene in terms of volume [4], so this has been used in this work as a model reactant for polyolefins. Furthermore, our previous results show that the deactivation of polypropylene (PP) is relatively similar to that of HDPE in the simultaneous pyrolysis–cracking [37]. The HDPE is supplied by Dow Chemical (Tarragona) with the following properties: molecular weight, 46,200 g mol$^{-1}$; polydispersity, 2.89; density, 940 kg m$^{-3}$ and higher heating value, 43 MJ kg$^{-1}$.

The sequenced pyrolysis–cracking unit used in this study has been shown and explained before [13]. The pyrolysis was performed in a conical spouted bed reactor, and the catalytic cracking of the volatiles of the former reactor was performed in a fixed bed reactor set in-line (Fig. 1). The HDPE is fed continuously (1 g min$^{-1}$) into the conical spouted bed reactor by means of a solid feed system, which consists of a vessel equipped with a vertical shaft connected to a piston. The plant also has a gas feeding and mixing system and a gas preheater. The dimensions of the conical spouted bed reactor used are established according to previous hydrodynamic studies and ensure bed stability in a wide range of operating conditions [38,39]. The bed was made up of 50 g of sand and $N_2$ (5 L min$^{-1}$) was used to fluidize the bed. The $N_2$ flow rate used was 20% above that required for the minimum spouting velocity, which ensures a vigorous cyclic movement of sand particles (avoiding defluidization) and high heat and mass transfer rates (ensuring isothermal conditions).

The volatiles formed in the pyrolysis (mainly waxes as described later in Section 3.1) were fed in line to the catalytic fixed bed reactor. Due to the fact that coke deposition is not homogeneous along the fixed bed, the catalytic fixed bed was divided into three sections with the same amount of catalyst in each of them (2.67 g, the total bed was 8 g), to study the coke deposition in each axial position (Fig. 1). The maximum reaction time studied was 5 h or 300 g of HDPE fed.

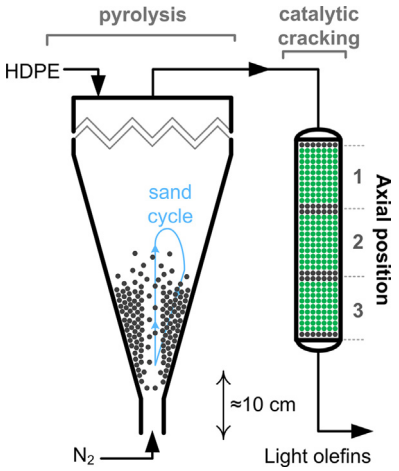


**Fig. 1.** Diagram of the unit used in the sequenced pyrolysis–cracking of HDPE. The latter step with the cracking catalyst bed divided into three axial positions A1–A3.

The reaction volatiles leaving the catalytic fixed bed reactor have been analyzed by a Varian 3900 gas-chromatograph (GC) connected online to the reactor by means of an isothermal pipe at 280 °C to avoid the condensation of the heavy products. Cyclohexane, which has been fed into the product stream at the outlet of the catalytic bed reactor, has been used as an internal standard to validate the mass balance. The non-condensable gases have been analyzed by a Varian 4900 micro gas-chromatograph. Liquid and gaseous products have been identified by means of a GC-MS spectrometer (Shimadzu 2010-QP2010S) and a micro GC–MS spectrometer (Agilent 5975B), respectively.

### 2.2. Catalyst

Zeolite HZSM-5 has been supplied in ammonium form (Zeolyst International, $SiO_2/Al_2O_3 = 30$). Therefore, prior to agglomeration it has been calcined at 550 °C to obtain the acid form. The zeolite (25 wt%) is agglomerated by wet extrusion with bentonite (Exaloid, 30 wt%) and α-alumina (Martinswerk, 45 wt%) previously calcined at 1100 °C. After agglomeration, the extrudates are dried at room temperature for 24 h, sieved in the range of 1–2 mm and followed by a second drying step at 110 °C for 24 h. Finally, the catalyst is calcined at 575 °C for 2 h, with a ramp of 5 °C min$^{-1}$ to reach this temperature, in order to eliminate the strong acid sites (hydrothermally unstable).

**Table 1**
Main properties of the zeolite and the catalyst.

| Property | Zeolite | Catalyst |
|---|---|---|
| BET surface area (m$^2$ g$^{-1}$) | 497 | 182 |
| Micropore[1] area (m$^2$ g$^{-1}$) | 385 | 98 |
| Mesopore[2] volume (cm$^3$ g$^{-1}$) | 0.07 | 0.26 |
| Pore volume distribution[3] (%) | 65/35/0 | 5/27/68 |
| Average pore diameter (Å) | 16.1 | 84 |
| Total acidity (μmol $NH_3$ g$^{-1}$) | 608 | 142 |
| Average acid strength (kJ (mol $NH_3$)$^{-1}$) | 150 | 150 |
| Acid distribution[4] (%) | 34/52/14 | 34/52/14 |

[1] $d_p$ < 20 Å.
[2] 20 Å < $d_p$ < 500 Å.
[3] $d_p$ < 20 Å/20 Å < $d_p$ < 500 Å/$d_p$ > 500 Å.
[4] $T$ < 280 °C; 280 °C < $T$ < 420 °C; $T$ > 420 °C.

Table 1 shows the main physical and acid properties of the active phase and the catalyst. The physical or structural properties of the catalyst (BET surface area, pore volume and pore size distribution) were measured using Micromeritics ASAP 2010. These properties are determined by adsorption–desorption of $N_2$ (Air liquid, purity 99.9995%) at −196 °C. The experimental procedure consists of degassing the sample for approximately 8 h at 150 °C to remove impurities, followed by an adsorption–desorption of $N_2$. The surface area was calculated using the BET method, the micropore diameter is considered $d_p$ < 20 Å, and the average pore diameter was calculated using the BJH method.

The acid properties of the catalysts have been determined by $NH_3$ adsorption–desorption: the values of total acidity and average acid strength have been obtained by monitoring the differential adsorption of $NH_3$ simultaneously by calorimetry and thermogravimetry in a Setaram TG-DSC 111 and the curve for temperature programmed desorption of $NH_3$ has been obtained by connecting a Blazer Instruments mass spectrometer (Thermostar) on-line to a Setaram TG-DSC 111. The zeolite surface properties are not impaired by the agglomeration with bentonite and the contribution is evident in the matrix area, increasing the meso- and macroporous structure. The acidic properties are reduced by a quarter by diluting of the zeolite in the catalyst, so it is necessary to indicate the null contribution of the acid sites in the matrix.

The nature of the acid sites has been studied by Fourier transform infrared (FTIR) spectroscopy in a Nicolet 6700 (Thermo) spectrophotometer. The samples of spent catalysts (20 mg) have been pelletized applying pressure equivalent to 10 t cm$^{-2}$ for 10 min. The catalyst has been heated to 450 °C with a 5 °C min$^{-1}$ ramp under vacuum for about 90 min, to clean the surface and remove impurities. After that, the temperature is stabilized at 150 °C, successive pulses of pyridine (Sigma-Aldrich, 99.8%) are performed, under a vacuum at 150 °C, for 30 min to remove physisorbed pyridine, and the corresponding spectrum is recorded. These steps have been repeated until the saturation of the sample.

### 2.3. Coke characterization

The amount of coke deposited on the catalyst has been measured by combustion of a sample taken from the fixed bed reactor. It should be noted that the coke deposited on the catalyst is subjected in the reactor to a stream of $N_2$ of 5 L min$^{-1}$ (at room conditions) at 500 °C, which eliminates the volatiles that do not contribute to catalyst deactivation. The experiments has been performed in a thermobalance TGA Q5000TA (Thermo Scientific) following the procedure: (1) scan of the sample with $N_2$ stream to remove impurities; (2) combustion with air at 550 °C with a temperature ramp of 5 °C min$^{-1}$ followed by isothermal conditions for 90 min (to ensure complete combustion of coke); (3) the sample has been cooled with a ramp of 15 °C min$^{-1}$ to 250 °C.

The TEM images have been obtained by means of transmission electron microscopy (Phillips CM200) with the aid of a Supertwin lens (point resolution of 0.235 nm) equipped with an EDX (energy-dispersive X-ray spectroscopy) system of microanalysis with a resolution of 137.4 eV.

The nature of bonds vibration has been determined by FTIR spectroscopy on a Nicolet 6700 spectrophotometer (Thermo). The deactivated catalyst sample (3 mg) has been pelletized with KBr (300 mg, purity >99%) applying a pressure equivalent to 10 t cm$^{-2}$. The sample has been degassed at 100 °C for 1 h. Then, air is allowed to pass through the chamber with a flow-rate of 60 mL min$^{-1}$ and temperature is raised linearly at 5 °C min$^{-1}$ to 550 °C, maintaining this temperature for 1 h. Simultaneously, the signal of $CO_2$ ($m/z$ = 44) is recorded on a mass spectrometer (OmniStar ThermoStar GDS 320 Pfeiffer Vacuum).

Raman spectroscopy has been performed in a Renishaw confocal microscope using two excitation beams: 514 nm and 785 nm wavelength, and subtracting the fluorescence caused by coke. The measurements were taken over 3–5 mg of spent catalyst, performing at least 3 analyses at different positions and reducing the exposure to air to avoid coke oxidation.

The nature of the coke has been measured by $^{13}$C CP-MAS NMR. $^{13}$C spectra have been carried out in a double resonance probe CP-MAS (Cross Polarization Magic Angle Spinning) with 7 mm rotors and the samples have been rotated at 10 kHz. The pulse sequence used was $^{13}$C CP-MAS standard Bruker DXR 400 WB PLUS (9.40 T), the frequency of 79.5 MHz, a spectral width of 30 kHz, contact time 2 ms and a waiting time of 5 s.

## 3. Results and discussions

### 3.1. Product yields in the steps of pyrolysis and catalytic cracking

The conversion of HDPE in the pyrolysis reactor is complete, and the products obtained have been grouped into six different lumps: light olefins ($C_{2-4}$), light alkanes ($C_{1-4}$), aromatics ($C_{6-11}$, mostly single-ring), $C_{5-11}$ aliphatics (non-aromatics), $C_{12-20}$ aliphatics (non-aromatics) and waxes ($C_{21+}$). Coke has not been considered in the mass balance, given that in all cases its yield is lower than 0.1 wt%. The product yields in the pyrolysis of HDPE are: light olefins, 0.42 wt%; light alkanes, 0.68 wt%; aromatics, 0.11 wt%; $C_{5-11}$ aliphatics, 10.9 wt%; and $C_{12+}$ aliphatics, 87.0 wt% (10.9 wt% of $C_{12-20}$ aliphatics and 67 wt% of waxes). This stream, composed mainly of waxes whose composition is detailed elsewhere [40], leaves the first reactor and is fed into the second reactor or cracking step.

Fig. 2 displays the effect of the space time (graph a) and reaction time on stream (TOS, graph b) on the product distribution obtained in the catalytic cracking. $C_{12-20}$ hydrocarbons and waxes ($C_{21+}$) have been grouped in this figure since the yield of waxes is lower than 1 wt%. The results evidence the efficiency of the HZSM-5 zeolite for transforming $C_{12+}$ hydrocarbons into lighter hydrocarbons, and particularly into light olefins. The composition of the gas phase throughout space time depicted in Fig. 2a has been obtained using different amounts of catalyst in the reactor, and would be useful to compare the composition of the coke deposited on the catalyst at different positions. Fig. 2b shows that the catalyst has a high selectivity of light olefins even when TOS is 5 h. However, it is noteworthy that the yield of light olefins decreases slightly (from 57.9 wt% at zero time down to 49.5 wt% at 5 h), as well as the yield of $C_{6-11}$ aromatics (from 10.2 wt% to 7.3 wt%). Furthermore, the yield of other fractions increases significantly over the 5 h on stream: $C_{5-11}$ non-aromatic compounds, from 15.2 wt% to 21.3 wt% and especially the $C_{12+}$, from 5.3 wt% to 12 wt%. These results are explained by the formation of coke on the catalyst, which deactivates the acid sites of the catalyst.

Based on the results in Fig. 2 and extrapolating the yields, it has been estimated that the catalyst deactivation after 5 h is equivalent to a decrease in space time from 8 $g_{cat}$ min $g_{HDPE}{}^{-1}$ to 6.7 $g_{cat}$ min $g_{HDPE}{}^{-1}$. Therefore catalyst deactivation gives way to a homogeneous loss of catalytic activity, not favoring any other side reaction. It should be noted that catalyst deactivation does not have the same effect on the individual yield of the three light olefins. The yields of propylene and ethylene decrease in the initial 40 min, from 32 wt% to 28.6 wt% and from 9.4 wt% to 6.8 wt%, respectively. However, the yield of butene increases from 16.5 wt% to 18.2 wt% in the same period. Between 40 min and 5 h, the yields of propylene and ethylene decrease slightly (from 28.6 wt% to 25.5 wt% and from 6.8 wt% to 4.9 wt%, respectively), whereas the yield of butenes remains almost constant. This effect is explained by the initial coke

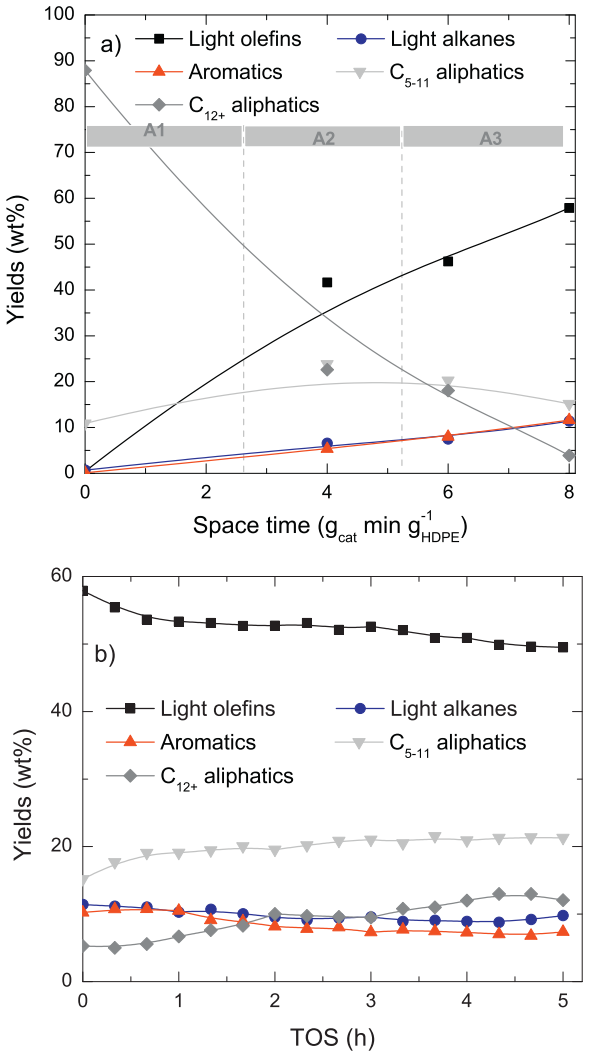


**Fig. 2.** Evolution of product yields with the space time (a) and TOS (b), the later graph using a space time of 8 $g_{cat}$ min $g_{HDPE}^{-1}$, at 500 °C.

deposition on catalyst strong acid sites, which have great influence on oligomerization–cracking reactions of branched olefins [41].

### 3.2. Deterioration of the catalytic properties

#### 3.2.1. Physical properties

Fig. 3 displays the $N_2$ adsorption–desorption isotherms of fresh and deactivated catalyst for three axial positions and two different TOS (2 h and 5 h). It should be noted that as TOS or axial position increases the catalyst loses more micropores, which is observed in the lower volume adsorbed at low partial pressures ($P/P_0 < 0.2$). Besides, the characteristic hysteresis of mesopores is narrower when TOS or axial position increases, showing that the catalyst loses more mesopores as both variables increase. However, the amount of macropores is not affected by TOS or axial position, being the volume adsorbed at high partial pressures similar for all catalysts studied.

Fig. 4 displays the evolution of catalyst physical properties (BET surface area and micropore area) with TOS for the three axial positions in the catalytic reactor. The BET surface area drops 46% in the axial position A1 after 5 h, whereas axial positions A2 and A3 lose 40%. The micropore area undergoes similar decay in the three axial positions, decreasing from 98 $m^2\,g^{-1}$ to approximately 50 $m^2\,g^{-1}$. Therefore, the blocking of micropores caused by coke is practically

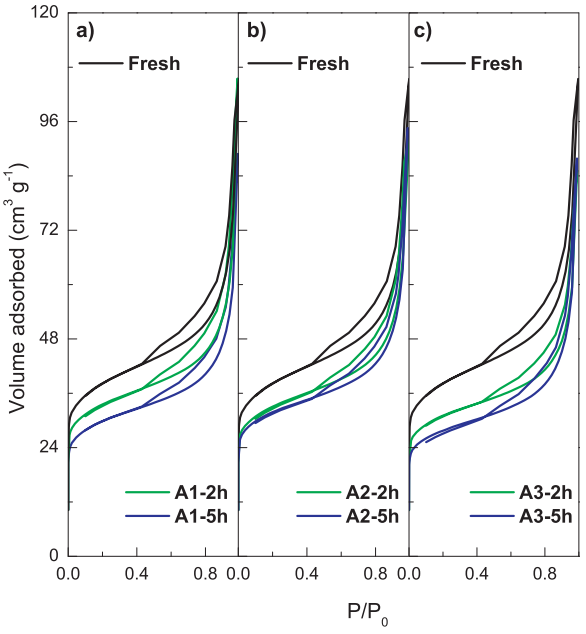


**Fig. 3.** Adsorption isotherms of the deactivated catalyst in axial positions A1–3, after TOS = 2 and 5 h de TOS. Conditions: 500 °C; space time (after A3), 8 $g_{cat}$ min $g_{HDPE}^{-1}$.

independent of the axial position, and the differences in BET surface area deterioration are due to losses of meso- and macroporous surface. Besides, it should be noted that the average pore diameter of the catalyst increases with TOS due to the blockage of the micropores and the higher relative contribution of meso- and macropores of the catalyst. Furthermore, deterioration of the surface properties is severely affected in the first hour of reaction in all positions. However, the deterioration of surface properties after this period is less pronounced, indicating that the catalyst is in a pseudo-steady deterioration state.

#### 3.2.2. Acid properties

Infrared spectroscopy of adsorbed pyridine is used to distinguish and quantify the amount of Brønsted and Lewis acids

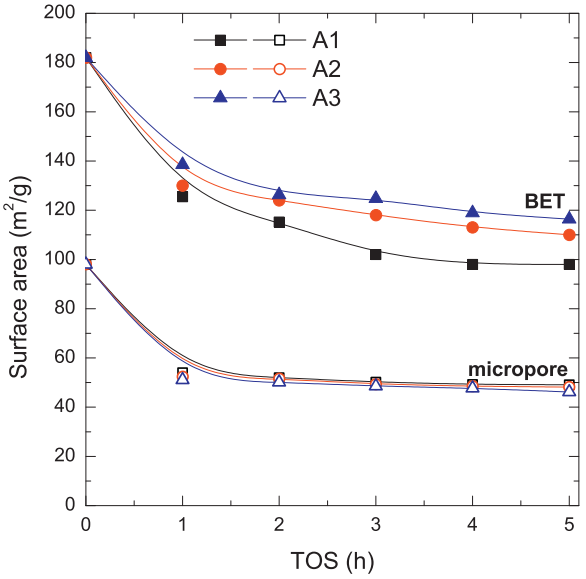


**Fig. 4.** Evolution of surface area with the TOS: BET area and micropore area. The deactivated catalyst in each axial position has been used in the following reaction conditions: 500 °C; space time (after A3), 8 $g_{cat}$ min $g_{HDPE}^{-1}$.

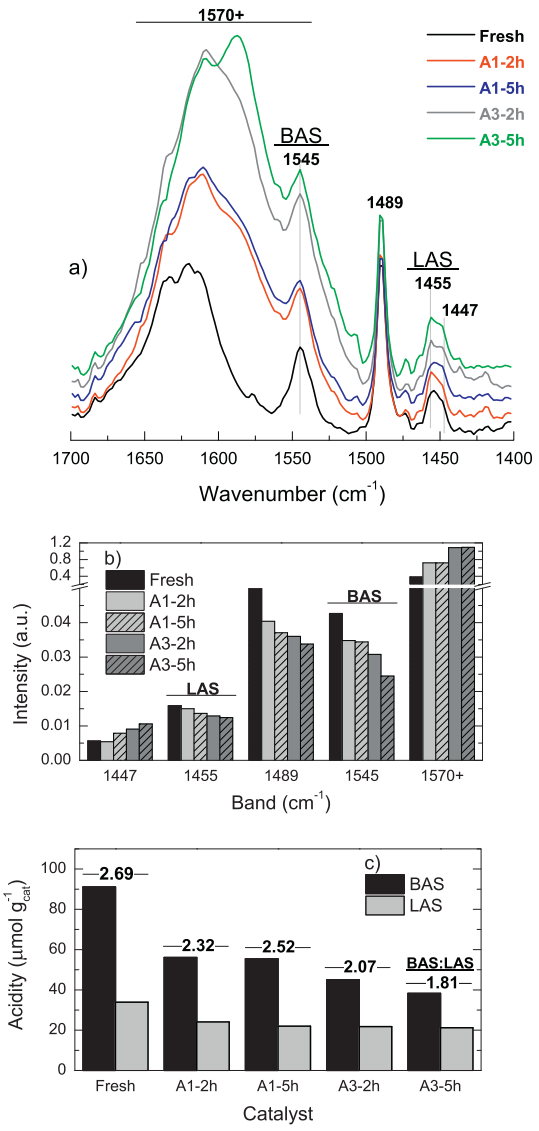


**Fig. 5.** Evolution of FTIR bands corresponding to pyridine adsorbed on the fresh and deactivated catalysts: (a) FTIR spectra, (b) deconvolution area of the peaks indicated in Fig. 4(a), and (c) concentration of acid sites.

sites. Fig. 5a shows the adsorption spectra at 150 °C in the region 1700–1400 $cm^{-1}$ at different axial positions and different TOS. Two bands distinguish the acid sites: Brønsted acid sites (BAS) at 1545 $cm^{-1}$ and Lewis acid sites (LAS) at 1455 $cm^{-1}$. The band at 1489 $cm^{-1}$ is due to the interaction between both types of acid sites, and the band at 1447 $cm^{-1}$, close to the vibration band of Lewis sites, corresponds to physisorbed or weakly bonded pyridine with LAS [42]. For wave numbers greater than 1570 $cm^{-1}$, several vibrational bands merge within the same region including coke, making identification difficult: conjugated double bonds at 1610 $cm^{-1}$, polycyclic aromatics at 1580 $cm^{-1}$ and others interactions of acid sites with pyridine.

Fig. 5b compares intensities of the different bands described in Fig. 5a, with intensities having been obtained by deconvolution in different Gaussians peaks. It can be observed that BAS as well as LAS band intensity decreases when axial position or TOS increase, whereas the intensities of bands associated with coke increase.

Fig. 5c shows the concentration (in mol $g^{-1}$) and the ratio ($B$:$L$) of BAS and LAS, which have been calculated according to molar extinction coefficients ($\varepsilon_B$ = 1.67 cm $mol^{-1}$ and $\varepsilon_L$ = 2.22 cm $mol^{-1}$) calculated by Emeis [43]. The total acidity of the fresh catalyst is

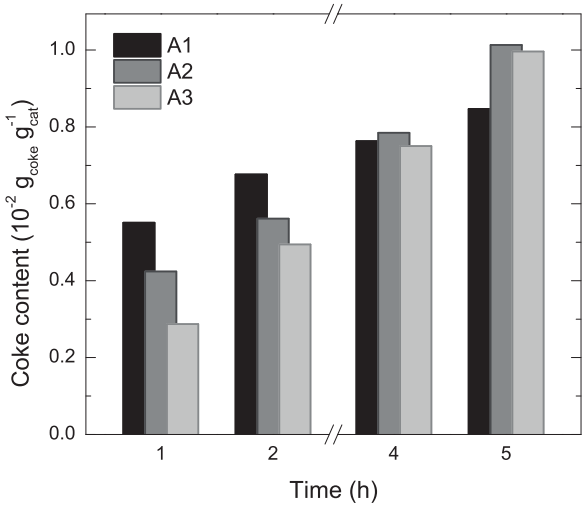


**Fig. 6.** Evolution of coke content with the TOS at different axial positions in the reactor. Conditions: 500 °C; space time (after A3), 8 $g_{cat}$ min $g_{HDPE}^{-1}$.

125 (μmol pyridine) $g^{-1}$: 91.1 (μmol pyridine) $g^{-1}$ corresponds to BAS and 33.9 (μmol pyridine) $g^{-1}$ to LAS ($B$:$L$ = 2.69). BAS of the catalyst decreases as TOS increases, especially in the axial position A3, where its value decreases by 58% after 5 h of reaction. However, LAS concentration remains almost constant (22 (μmol pyridine) $g^{-1}$) as TOS or axial position increase, although it decreases in relation to the fresh catalyst. Thus, $B$:$L$ ratio decreases in relation to the fresh catalyst, obtaining the lowest value ($B$:$L$ = 1.81) at 5 h and in the axial position A3.

Therefore, it can be concluded that the coke deposited at low TOS values blocks LAS and BAS, leading to a decrease in the concentration of both acid sites at the beginning of the reaction. Nevertheless, as TOS increases the coke is deposited preferentially blocking BAS and this blockage is more severe as the axial position is increased.

### 3.3. Properties and amount of coke

#### 3.3.1. Evolution of coke formation

Fig. 6 shows the evolution of coke content on the catalyst with the TOS in each axial position. Coke content has been obtained by combustion (TG-TPO). The coke content on the catalyst is always less than 1 wt%, which is much lower than that necessary to block the micropores of the zeolite [44]. The relatively low amount of coke deposited explains the moderate deactivation observed (Fig. 2b), whereas the deterioration of physical and acid properties is significant (Figs. 4 and 5).

The HZSM-5 zeolite unique features play a significant role in quenching deactivation, since its acid properties and pore network in particular, favor the removal of coke precursors, whereas the formation exclusion of bulky hydrocarbons [28,32,45]. The agglomeration of the zeolite crystals with alumina and bentonite generates an external structure, with meso and macropores, where coke deposits and growths, reducing deposition in the mouth of crystalline channels of the zeolite [46]. Moreover, the reaction system used also contributes to minimizing coke deposition since the high $N_2$ flow rate has a stripping effect on the coke precursors towards the exterior of the zeolite crystals, with a limited residence time of these precursors in the catalytic reactor, which hinders the growth of coke. As observed in Fig. 6, the coke content deposited in the first hour follows the trend A1 > A2 > A3. An increase in TOS gives way to an increase in the amount of coke deposited on the catalyst, being this growth more pronounced as axial position is higher. Although the amount of coke deposited at the reaction initial period is higher in the axial position A1, the rate of coke formation is higher in the

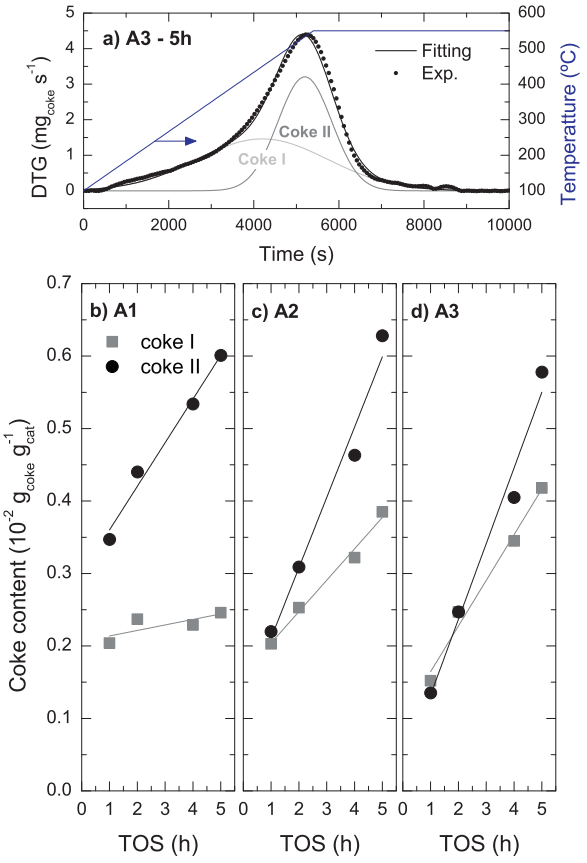


**Fig. 7.** (a) Deconvolution in two types of coke (I, II), A3–5 h. (b)–(d) Evolution of the coke I and II content with the TOS in the three axial positions of the reactor. Conditions: 500 °C; space time (after A3), 8 $g_{cat}$ min $g_{HDPE}^{-1}$.

axial position A3. Thus, for 5 h on stream the coke content is higher in A3 than in A1. The precursors of coke can be identified correlating coke formation with the composition of the gas phase in each axial position of the catalytic reactor (Fig. 2a), and also with the TOS.

### 3.3.2. Evolution of coke composition

The combustion profiles (TG-TPO) show two combustion peaks, one in the 450–470 °C range and the other in the 520–530 °C range. Thus, the profiles have been deconvoluted in two Gaussian peaks in order to identify the two types of coke I and II, respectively. This procedure is used routinely in the literature and has been previously applied for analyzing the coke deposited on the acid catalysts during the simultaneous pyrolysis–cracking [29,37]. The two types of coke are associated with different coke composition and location on the catalyst: coke I has higher H/C ratio (less evolved) and is deposited less selectively in the macroporous and mesoporous catalyst structure; coke II has lower H/C ratio, deposits in the micropores (undergoing diffusional limitations for growing, combustion or desorption [47]) and outside the zeolite crystals (associated with a more developed coke; graphitic and aromatic).

Fig. 7a, shows the deconvolution in two Gaussians peaks, associated with coke I and coke II. Fig. 7b–d show that the formation rate of both types of coke is linearly dependent on the TOS, which has already been observed in the simultaneous pyrolysis–cracking of HDPE and PP [37]. These results indicate that coke formation rate (slope of the lines) is constant in the three axial positions of the catalytic reactor, and its value could be linked to the composition of the gas phase.

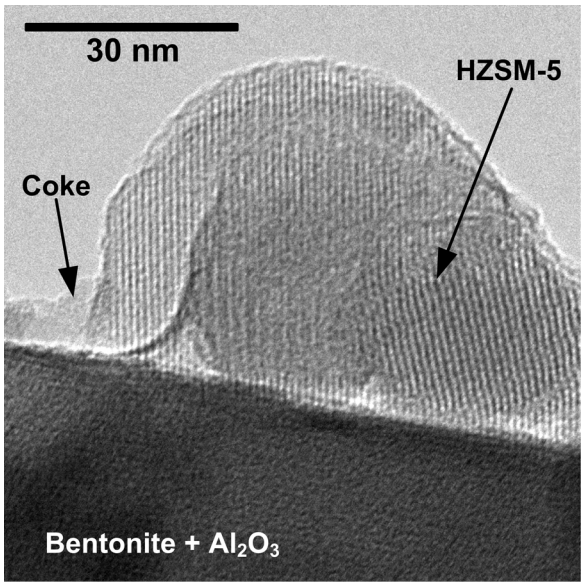


**Fig. 8.** TEM image of the spent A3–5 h catalyst (300 g of HDPE fed in the reactor).

Fig. 8 shows a TEM image of the catalyst A3–5 h as an example. Most of the features of the catalyst can be distinguished: a crystal of zeolite HZSM-5 and its pore network; the matrix of binder and filler (bentonite-$Al_2O_3$); and the external coke. As can be observed in Fig. 8, internal coke (within the pores of the zeolite) is difficult to be identified by TEM analysis. However, TEM images indicate the precise location of the external coke.

Fig. 9 displays the temperature programmed combustion of the catalyst located in axial position A3 and used 2 h and 5 h on stream. The evolution of the differential $CO_2$ signal has been monitored by MS and the bands of conjugated double bonds (dienes), polycyclic aromatic hydrocarbons (PAH) and aliphatic by FTIR spectroscopy. The $CO_2$ signal is very similar to that in the TG (not shown in this work), with two combustion steps corresponding to coke I and II. The characteristic bands of coke (they have not been observed in the fresh catalyst) in the FTIR spectra of the deactivated catalysts are [34,46–48]: 1610 $cm^{-1}$, diene; 1580 $cm^{-1}$, polycyclic aromatic hydrocarbon (PAH), also called coke band; 2930 $cm^{-1}$, aliphatic $-CH_2$, –CH; and 2960 $cm^{-1}$ $-CH_3$ terminal aliphatic groups.

Similarly to the $CO_2$ signal, the FTIR band signals also show two thermal events corresponding to: (i) combustion of aliphatic groups (–CH, $-CH_2$ and $-CH_3$) with a maximum at 320 °C (coke I), (ii) combustion of poly-aromatics and dienes, with a maximum at temperatures of 525 °C (coke II). Consequently, the difference between coke I and II is based on the coke composition: coke I is mainly aliphatic, and coke II is more aromatic. Coke II has two clearly differentiated contribution events: (i) aromatic coke deposited on the inside of the micropores and (ii) polycyclic aromatic coke deposited on the outside of the zeolite. It should be noted that in the 100–220 °C range the $CO_2$ signal is unchanged, whereas the FTIR signal shows the transformation of aliphatic compounds into aromatic and dienes during the combustion. This fact is related to two competing processes during TPO: (i) thermal cracking and dehydrogenation, and (ii) combustion above 220 °C.

FTIR band intensities of molecular bond vibrations characteristic of the coke deposited on the catalyst in the three axial positions are shown in Fig. 10. The coke deposited in axial position A1 after 2 h of reaction is predominantly composed of aliphatic long chains, with the FTIR intensity of intermediate $-CH_2$ and –CH groups being two times higher than the remaining bands. As TOS increases, the coke deposited in the axial position A1 develops towards a more

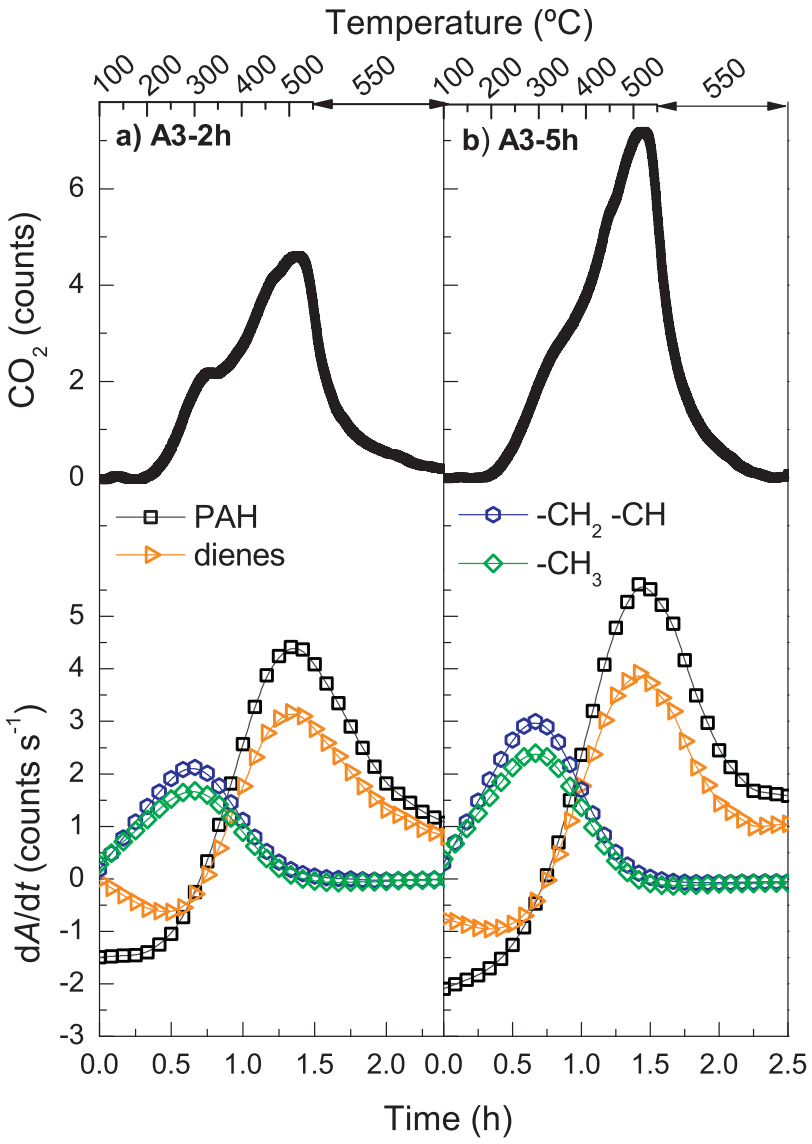


**Fig. 9.** MS and FTIR-TPO profiles for deactivated catalyst in the axial positions A3, (a) TOS = 2 h and (b) TOS = 5 h. Conditions: 500 °C.

structured and aromatic coke, which can be explained by the aging undergone at 500 °C [48,49]. In axial position A2 and A3, the coke deposited is more developed than that deposited in A1 for all values of TOS.

The aforementioned differences in coke composition and formation rate in each axial position are linked to the composition of the gas phase. If the gas phase contains $C_{12+}$ aliphatics, as happens in axial position A1, the nature of the coke formed is largely aliphatic. However, if the gas phase contains mainly light olefins, as happens in axial position A2, and particularly in A3, the coke formed is mainly aromatic. It should be noted that the aliphatic coke formed by wax degradation in the axial position A1 evolves towards aromatic coke when reaction temperature and TOS are sufficiently high. This result is due to several reactions: dehydrogenation, cyclization and hydrogen transfer among others. [47,50]

Fig. 11 shows the Raman spectra in the 1000–2000 $cm^{-1}$ region, corresponding to bands of coke deposited on the catalyst in the axial positions A1 and A3, for times on stream of 2 h and 5 h. The band at 1350 $cm^{-1}$ is attributed to the disordered aromatic structures (*D*) and the band of 1600 $cm^{-1}$ is attributed to aromatic structures and ordered graphitic (*G*) [51–54]. Fig. 11 also summarizes the values of the *D*/*G* ratio, which has been correlated to the growth phases of carbonaceous materials by Tuinstra and Koenig [55] and by Robertson [56]. The *D*/*G* ratio increases with TOS, particularly in the axial position A1, as a consequence of an increase in the particle size of the coke. The coke deposited in the axial position A3 has a substantially lower value of *D*/*G* compared to that of A1, indicating that the coke deposited in A1 is more disordered and amorphous.

Solid state $^{13}C$ NMR spectroscopy results are shown in Fig. 12 for the axial positions A1 and A3, for 2 h and 5 h. Two different bands are distinguished [34,54,55]: (i) aliphatic carbon nuclei in the 10–40 ppm range; and (ii) aromatic carbon nuclei in $sp^2$ hybridation at 129 ppm. The coke deposited in the axial position A1 after 2 h on stream has primarily aliphatic (85%) nature; long chains paraffins, with the most intense band at 32 ppm corresponding to intermediate groups $–CH_2$ and –CH. Interestingly, the coke deposited in the same axial position (A1) after 5 h on stream has been transformed into aromatics (82%). On the other hand, the coke deposited in the axial position A3 after 2 h on stream is of aromatic nature, and keeps this nature steadily with TOS. Consequently, the results of $^{13}C$ NMR support the same conclusions extracted from FTIR (Fig. 10) and Raman spectra (Fig. 11) regarding the structure and composition of the coke and their link to the axial position and the composition of the gas phase.

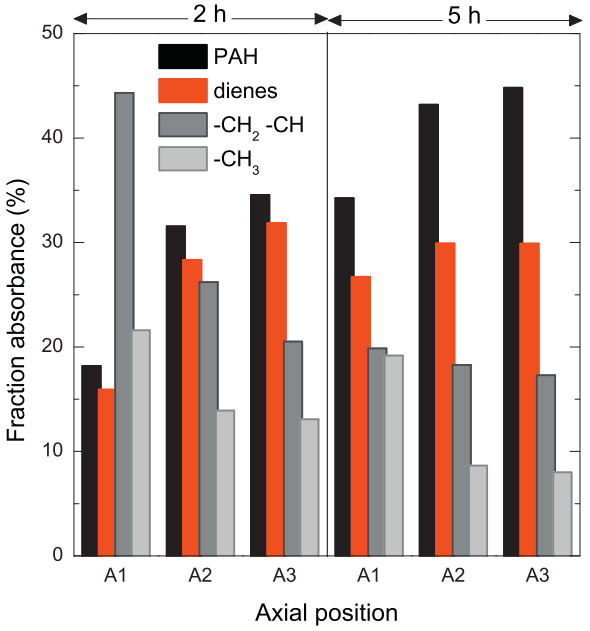


**Fig. 10.** Fraction of FTIR-absorbance bands present in the deactivated catalyst in axial positions A1–3, after TOS = 2 and 5 h de TOS. Conditions: 500 °C; space time (after A3), 8 $g_{cat}$ min $g_{HDPE}^{-1}$.

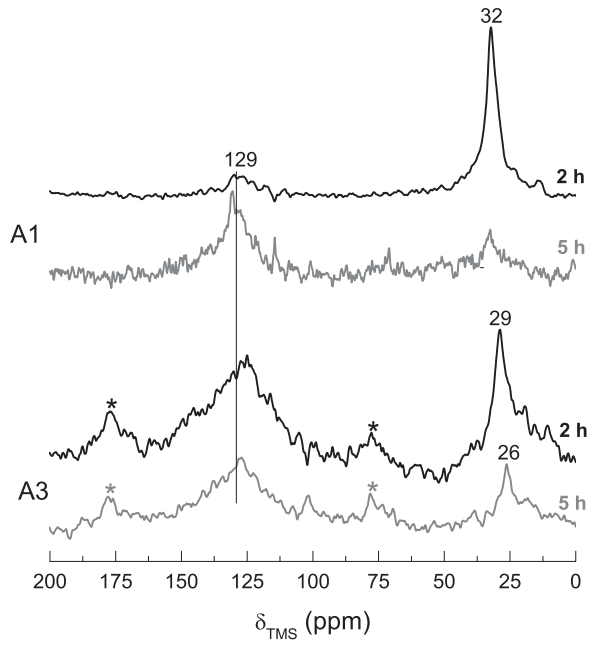


**Fig. 12.** Profiles of $^{13}C$ CP-MAS NMR of the deactivated catalyst in axial positions A1 and A3, and TOS = 2 and 5 h. Conditions: 500 °C; space time (after A3), 8 $g_{cat}$ min $g_{HDPE}^{-1}$.

### 3.4. Controlling coke formation

The results presented here concerning the coke deposited in the second step of the sequenced pyrolysis–cracking have been compared with those obtained for the simultaneous pyrolysis–cracking process described before [29,32]. The composition of the coke formed in both strategies (analyzed by FTIR, FTIR-TPO, Raman and $^{13}C$ NMR) is very similar. However, the study carried out in sequenced steps provides relevant information regarding the kinetics of catalyst deactivation and, particularly, for the identification of coke precursors. Fig. 13a shows the "initial" coke I and II deposited on the catalyst in the simultaneous pyrolysis–cracking [37] and in the 3 axial positions of the sequenced pyrolysis–cracking. These values have been obtained by extrapolating the rates of coke formation (evolution slopes of coke content vs. TOS) at zero time on stream. Fig. 13b shows the average formation rates of each types of coke throughout 5 h on stream for the simultaneous

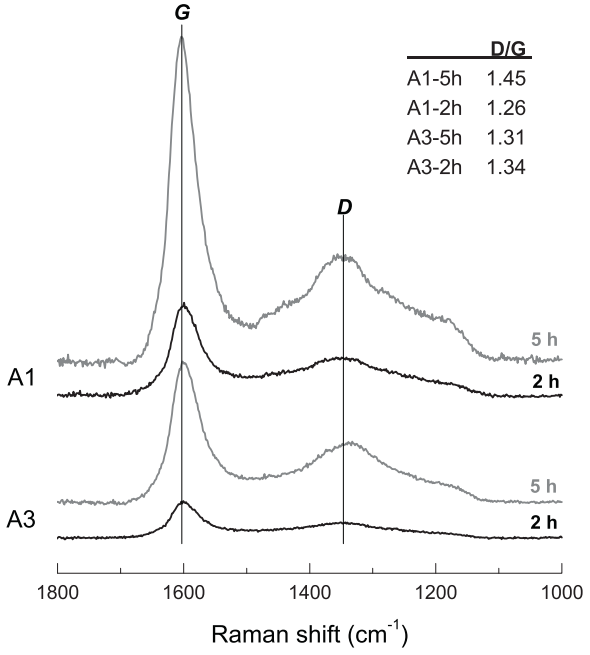


**Fig. 11.** Raman spectra (region 1000–1800 $cm^{-1}$) of the deactivated catalyst in axial positions A1 and A3, and TOS = 2 and 5 h. Conditions: 500 °C; space time (after A3), 8 $g_{cat}$ min $g_{HDPE}^{-1}$.

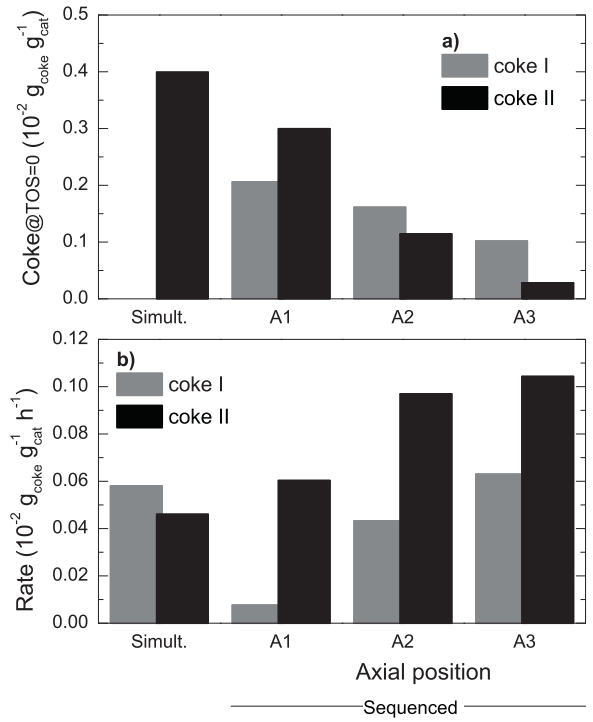


**Fig. 13.** Comparison of the (a) initial coke deposited interpolating at TOS = 0, and (b) coke formation rate in the simultaneous and sequenced pyrolysis–cracking of HDPE. Conditions: 500 °C.

pyrolysis–cracking [37] and for the 3 axial positions of the sequenced pyrolysis–cracking.

Is observed in Fig. 13a for the simultaneous process, the coke formed in the initiation period is only coke II and its value is higher than that in the sequenced process (in each axial position of the catalytic reactor). This result is explained by the reaction features of the simultaneous process; the catalyst is exposed simultaneously to melted HDPE, waxes and light olefins, and all of these reactants drive to the selective formation of coke II in the first hour on stream. Furthermore, in the sequenced process the catalyst is exposed to lighter products not including HDPE, and the gas phase composition varies severely along the axial position in the reactor; from waxes to light olefins. Fig. 13a shows that in the reactor initial section (axial position A1), the deposition of coke II is more significant during the initiation period. During the inition period, the coke formation is greater in the simultaneus process and the axial position A1 (Fig. 13a). On the contrary and during the steady coke formation period, the coke formation rate is higer in axial position A2 and A3. This effect is due to the presence of melted HDPE and waxes in contact with the catalyst in the simultaneous process, which lead to a faster formation of coke, and particularly coke I, which is more aliphatic. In the sequenced process, the trend in coke formation rate is A3 > A2 > A1, which clearly evidences that light olefins are coke precursors, especially of coke II (this is why the formation rate of coke II is always greater than that of coke I in the sequenced process).

Consequently, these results clarify the role of the waxes (long chain hydrocarbons) and light olefins as precursors of coke formation, and understanding the evolution along the catalyst bed of each type of coke formed from waxes or light olefins. The aliphatic coke I is originated from the waxes on the outside of the zeolite crystals. For the initial hours on stream (initiation period), this coke I evolves towards condensed aromatic structures or coke II. Excluding the initiation period, waxes are less significant for coke formation compared with light olefins. Olefins allow a constant condensation rate of hydrocarbons (steady coke formation) on the acid sites of the zeolite, which block the micropores or leave the zeolite structure and oligomerize as polycyclic aromatics. Both types of condensed coke are regarded as coke II.

The aforementioned results show that coke deposits differently along the axial position in the catalytic reactor (sequenced process) due to the difference in composition of the gas phase. This evidence involves great potential to use strategies to control coke formation and deactivation. Thus, a hybrid (cascade) catalyst bed enhances the stability of the process by increasing the mesopore area of the catalyst at the initial section of the reactor, and lessening the acidity of the catalyst near the reactor outlet. The mesopore area might be increased using different proportions of binder/filler/zeolite, or desilicating the zeolite [57,58]. Acidity is decreased using zeolites with higher $SiO_2/Al_2O_3$ ratio or doping with K or P [29,59].

For futures studies of deactivation modeling in this process, it is useful to establish a relation between coke deposition and the concentration of precursors in the gas phase. The results obtained in this study open the possibility to propose a kinetic equation dependent on the component concentration, taking as an example the deactivation models of methanol transformation to hydrocarbons [45,60]. Two periods could be assumed: (1) initiation period within the first hour on stream and (2) steady coke formation period occurring after the first hour on stream. In the initiation period, the deactivation rate depends on the wax concentration in the gas phase. In the steady coke formation period, coke deposition is due to the condensation of light olefins. Therefore, the concentration of light olefins in the gas phase should be considered in the deactivation equation.

## 4. Conclusions

The sequential pyrolysis–cracking of waste HDPE is an attractive process for light olefin production, given that one of the main drawbacks of this valorization route is catalyst deactivation. In this work, we have demonstrated that HZSM-5 zeolite catalyst can be used to control catalyst deactivation. The relationship between the deactivation and the composition of the gas phase reveals that waxes and light olefins are the precursors of coke formation. Waxes deactivate the initial section of the catalytic reactor, particularly in the first hour on stream during the initiation period. As the concentration of light olefins increases with the space time or axial position, so does their condensation and oligomerization to form coke. Light olefins cause a period of steady coke formation with TOS.

The results of TG-TPO show two types of coke, the composition of which have been elucidated using FTIR-TPO and combining several spectroscopic techniques. Coke I has an aliphatic nature, stems mainly from the degradation of waxes and long chain paraffins, and it is located on the outside of the zeolite crystals on the mesoporous and macroporous structure of the binder and filler. Coke II has an aromatic nature, either monoaromatic within the pores of the zeolite or polyaromatic in the exterior of the zeolite pores, with its formation being according to: degradation of coke I and oligomerization and condensation of light olefins. Light olefins diffuse well inside the pores of the zeolite, making the deactivation caused by them more selective towards the blockage of the Brønsted acid sites. These deactivation pathways can be formulated in kinetic equations for the reactor design, and also for proposing novel strategies to control de deactivation in this process, i.e. using a cascade catalyst with tailored properties along the reactor (axial position).

These results evidence the great potential of the HZSM-5 zeolite to cope with coke deposition. This is a result of its unique intrinsic features: right balance of acidic sites in terms of strength and nature, and a pore network that favors the removal of coke precursors thanks to a high connectivity and the absence of cages in the network.

## Acknowledgments

The financial support of this work was undertaken by the Ministry of Science and Education of the Spanish Government (Project CTQ2010-19623), the Basque Government (Project IT748-13; BFI-2012-203), and the University of the Basque Country (UFI 11/39 UPV/EHU).

## References

[1] S.M. Al-Salem, P. Lettieri, J. Baeyens, Waste Manage. 29 (2009) 2625–2643.
[2] A.K. Panda, R.K. Singh, D.K. Mishra, Renewable Sustainable Energy Rev. 14 (2010) 233–248.
[3] J. Aguado, D.P. Serrano, J.M. Escola, Ind. Eng. Chem. Res. 47 (2008) 7982–7992.
[4] S. Kumar, A.K. Panda, R.K. Singh, Resour. Conserv. Recycl. 55 (2011) 893–910.
[5] E. Butler, G. Devlin, K. McDonnell, Waste Biomass Valor. 2 (2011) 227–255.
[6] P.T. Williams, E.A. Williams, J. Anal. Appl. Pyrolysis 51 (1999) 107–126.
[7] C. Berrueco, E.J. Mastral, E. Esperanza, J. Ceamanos, Energy Fuels 16 (2002) 1148–1153.
[8] J. Mertinkat, A. Kirsten, M. Predel, W. Kaminsky, J. Anal. Appl. Pyrolysis 49 (1999) 87–95.
[9] J. Aguado, D.P. Serrano, G.S. Miguel, J.M. Escola, J.M. Rodríguez, J. Anal. Appl. Pyrolysis 78 (2007) 153–161.
[10] A. Marcilla, M.I. Beltrán, R. Navarro, Appl. Catal., B 86 (2009) 78–86.
[11] J. Aguado, D.P. Serrano, G. San Miguel, M.C. Castro, S. Madrid, J. Anal. Appl. Pyrolysis 79 (2007) 415–423.
[12] D.S. Achilias, C. Roupakias, P. Megalokonomos, A.A. Lappas, V. Antonakou, J. Hazard. Mater. 149 (2007) 536–542.
[13] M. Artetxe, G. Lopez, M. Amutio, G. Elordi, J. Bilbao, M. Olazar, Chem. Eng. J. 207–208 (2012) 27–34.
[14] J. Walendziewski, M. Steininger, Catal. Today 65 (2001) 323–330.
[15] Y.H. Lin, M.H. Yang, J. Anal. Appl. Pyrolysis 83 (2008) 101–109.

[16] G. Grause, S. Matsumoto, T. Kameda, T. Yoshioka, Ind. Eng. Chem. Res. 50 (2011) 5459–5466.
[17] P.J. Donaj, W. Kaminsky, F. Buzeto, W. Yang, Waste Manage. 32 (2012) 840–846.
[18] M. Artetxe, G. Lopez, M. Amutio, G. Elordi, M. Olazar, J. Bilbao, Ind. Eng. Chem. Res. 49 (2010) 2064–2069.
[19] J. Makibar, A.R. Fernandez-Akarregi, I. Alava, F. Cueva, G. Lopez, M. Olazar, Chem. Eng. Process. 50 (2011) 790–798.
[20] M.J. San José, M. Olazar, F.J. Peñas, J.M. Arandes, J. Bilbao, Chem. Eng. Sci. 50 (1995) 2161–2172.
[21] G. Elordi, M. Olazar, G. Lopez, M. Artetxe, J. Bilbao, Ind. Eng. Chem. Res. 50 (2011) 6650–6659.
[22] G. Elordi, M. Olazar, G. Lopez, M. Artetxe, J. Bilbao, Ind. Eng. Chem. Res. 50 (2011) 6061–6070.
[23] G. Lopez, M. Artetxe, M. Amutio, G. Elordi, R. Aguado, M. Olazar, J. Bilbao, Chem. Eng. Process. 49 (2010) 1089–1094.
[24] G. Elordi, M. Olazar, G. Lopez, M. Amutio, M. Artetxe, R. Aguado, J. Bilbao, J. Anal. Appl. Pyrolysis 85 (2009) 345–351.
[25] W. Kaminsky, I.J.N. Zorriqueta, J. Anal. Appl. Pyrolysis 79 (2007) 368–374.
[26] P. Gaca, M. Drzewiecka, W. Kaleta, H. Kozubek, K. Nowinska, Pol. J. Environ. Stud. 17 (2008) 25–31.
[27] Z. Obali, N.A. Sezgi, T. Dogu, Chem. Eng. Commun. 196 (2009) 116–130.
[28] G. Elordi, M. Olazar, G. Lopez, P. Castaño, J. Bilbao, Appl. Catal., B 102 (2011) 224–231.
[29] G. Elordi, M. Olazar, M. Artetxe, P. Castaño, J. Bilbao, Appl. Catal., A 415–416 (2012) 89–95.
[30] F. Ates, N. Miskolczi, N. Borsodi, Bioresour. Technol. 133 (2013) 443–454.
[31] A. Angyal, N. Miskolczi, L. Bartha, I. Valkai, Polym. Degrad. Stab. 94 (2009) 1678–1683.
[32] P. Castaño, G. Elordi, M. Olazar, A.T. Aguayo, B. Pawelec, J. Bilbao, Appl. Catal., B 104 (2011) 91–100.
[33] N. Miskolczi, L. Bartha, G. Deak, Polym. Degrad. Stab. 91 (2006) 517–526.
[34] A. Marcilla, A. Gómez-Siurana, F.J. Valdés, Appl. Catal., A 352 (2009) 152–158.
[35] A. Marcilla, M.I. Beltrán, A. Gómez-Siurana, R. Navarro, F. Valdés, Appl. Catal., A 328 (2007) 124–131.
[36] P. Castaño, G. Elordi, M. Olazar, J. Bilbao, ChemCatChem 4 (2012) 631–635.
[37] P. Castano, G. Elordi, M. Ibanez, M. Olazar, J. Bilbao, Catal. Sci. Technol. 2 (2012) 504–508.
[38] M. Olazar, M.J. San José, A.T. Aguayo, J.M. Arandes, J. Bilbao, Ind. Eng. Chem. Res. 32 (1993) 1245–1250.
[39] M. Olazar, M.J. San José, S. Alvarez, A. Morales, J. Bilbao, Ind. Eng. Chem. Res. 43 (2004) 655–661.
[40] M. Arabiourrutia, G. Elordi, G. Lopez, E. Borsella, J. Bilbao, M. Olazar, J. Anal. Appl. Pyrolysis 94 (2012) 230–237.
[41] G. Zhao, J. Teng, Z. Xie, W. Jin, W. Yang, Q. Chen, Y. Tang, J. Catal. 248 (2007) 29–37.
[42] L.H. Ong, M. Dömök, R. Olindo, A.C. Van Veen, J.A. Lercher, Microporous Mesoporous Mater. 164 (2012) 9–20.
[43] C.A. Emeis, J. Catal 141 (1993) 347–354.
[44] A.T. Aguayo, P.L. Benito, A.G. Gayubo, M. Olazar, J. Bilbao, Stud. Surf. Sci. Catal. (1994) 567–572.
[45] A.T. Aguayo, A.G. Gayubo, J.M. Ortega, M. Olazar, J. Bilbao, Catal. Today 37 (1997) 239–248.
[46] J. Kim, M. Choi, R. Ryoo, J. Catal. 269 (2010) 219–228.
[47] M. Guisnet, P. Magnoux, Appl. Catal., A 212 (2001) 83–96.
[48] P. Magnoux, H.S. Cerqueira, M. Guisnet, Appl. Catal., A 235 (2002) 93–99.
[49] A.T. Aguayo, A.G. Gayubo, J. Ereña, A. Atutxa, J. Bilbao, Ind. Eng. Chem. Res. 42 (2003) 3914–3921.
[50] M. Guisnet, L. Costa, F.R. Ribeiro, J. Mol. Catal. A: Chem. 305 (2009) 69–83.
[51] C. Li, P.C. Stair, Catal. Today 33 (1997) 353–360.
[52] B.M. Vogelaar, A.D. van Langeveld, S. Eijsbouts, J.A. Moulijn, Fuel 86 (2007) 1122–1129.
[53] B. Guichard, M. Roy-Auberger, E. Devers, B. Rebours, A.A. Quoineaud, M. Digne, Appl. Catal., A 367 (2009) 1–8.
[54] A.T. Aguayo, P. Castaño, D. Mier, A.G. Gayubo, M. Olazar, J. Bilbao, Ind. Eng. Chem. Res. 50 (2011) 9980–9988.
[55] F. Tuinstra, J.L. Koenig, J. Chem. Phys. 53 (1970) 1126–1130.
[56] J. Robertson, Mater. Sci. Eng., R 37 (2002).
[57] A.G. Gayubo, A. Alonso, B. Valle, A.T. Aguayo, J. Bilbao, Appl. Catal., B 97 (2010) 299–306.
[58] F.L. Bleken, K. Barbera, F. Bonino, U. Olsbye, K.P. Lillerud, S. Bordiga, P. Beato, T.V.W. Janssens, S. Svelle, J. Catal. 307 (2013) 62–73.
[59] Y. Sun, S.M. Campbell, J.H. Lunsford, G.E. Lewis, D. Palke, L.M. Tau, J. Catal. 143 (1993) 32–44.
[60] P.L. Benito, A.G. Gayubo, A.T. Aguayo, M. Castilla, J. Bilbao, Ind. Eng. Chem. Res. 35 (1996) 81–89.